We are IntechOpen, the world's leading publisher of Open Access books Built by scientists, for scientists

6,900
Open access books available

185,000
International authors and editors

200M
Downloads

Our authors are among the

154
Countries delivered to

TOP 1%
most cited scientists

12.2%
Contributors from top 500 universities



WEB OF SCIENCE™

Selection of our books indexed in the Book Citation Index in Web of Science™ Core Collection (BKCI)

Interested in publishing with us?
Contact book.department@intechopen.com

Numbers displayed above are based on latest data collected.
For more information visit www.intechopen.com



8

Ultrasonic Grain Refinement of Magnesium and Its Alloys

M. Qian[1] and A. Ramirez[2]
[1]*The University of Queensland, School of Mechanical and Mining Engineering*
Australian Research Council (ARC) Centre of Excellence for Design in Light Metals
Brisbane QLD 4072
[2]*Aix-Marseille Université and CNRS, UMR 6242, IM2NP*
Campus de Saint Jérôme, Case 142, 13397 Marseille Cedex 20,
[1]*Australia*
[2]*France*

1. Introduction

Achievement of a uniform fine grain structure in cast magnesium (Mg) alloys is desired as it improves structural uniformity, reduces segregation and associated casting defects, enhances consistency in performance, and facilitates the solid-state forming of various wrought Mg products. Inoculation is a standard grain-refining practice for commercial cast alloys. However, many commercial alloy systems do not have an established inoculating agent or chemical grain refiner. In the context of Mg alloys, although aluminium-free Mg alloys can be readily grain-refined with zirconium (Emley, 1966; Qian & Das, 2006; Qian, 2006), it has proved difficult to grain-refine the more common Mg-Al based alloys by inoculation (StJohn et al., 2005; Qian & Cao, 2005). Alternative approaches to grain-refining these alloys are desirable.

Ultrasonic irradiation during solidification is one such alternative that has proved to be effective for Mg-Al based alloys, first demonstrated in the former USSR countries (Abramov, 1994; Eskin, 1998). It is also effective in grain-refining other metallic materials (Eskin, 1998; Jian et al., 2005; Jian et al., 2006a; Liu et al., 2007; Xu et al., 2008) and ice (Zhang et al., 2001). The recent renewed interest in the process for Mg alloys (Jian et al., 2006b; Ramirez & Qian, 2007; Zhang et al., 2007; Liu et al., 2008; Ramirez et al., 2008; Ramirez et al., 2009; Qian & Ramirez, 2009; Qian et al., 2009; Qian et al., 2010a) is driven by its potent grain-refining capability, ease of operation, and requirement for inexpensive equipment. In addition, the melt surface is left almost undisturbed during irradiation. As a result, there is little concern over contamination by oxidation. In fact, molten Mg and its alloys are particularly suited to ultrasonication for structural refinement, partially because of their low viscosity (η), where $\eta_{Mg} = 1.25 \times 10^{-3}$ N s m^{-2} at 651 °C (Brandes & Brook, 1992), being almost the same as that of water, where $\eta_{Water} = 1.002 \times 10^{-3}$ N s m^{-2} at 20°C (Lide, 2001). Low viscosity implies low attenuation (see Eq.(2)), which is important for the structural refinement of a large volume of melt. However, the lack of fundamental understanding of the ultrasonic refining process has largely restricted its development and application.

This chapter reviews the current understanding of ultrasonic grain refinement (UGR) of Mg and its alloys and discusses issues that are central to UGR, including the characteristics of UGR of Mg alloys, the dependence of UGR on solute or alloy chemistry, the attenuation in liquid Mg alloys, and the mechanisms of UGR.

2. Ultrasonic irradiation

Ultrasonic irradiation, in general, can be divided into direct and indirect ultrasonication depending on the melting point of the liquid and its chemical reactivity with the sonotrode, also referred to as ultrasonic horn or radiator. Fig. 1 illustrates the two approaches (Qian et al., 2009). The sonotrode is often made of titanium (Ti-6Al-4V) or stainless steel or niobium because of their high efficiency in transmitting ultrasound, chemical inertness to many liquids, dimensional stability, and mechanical performance at elevated temperatures. Dimensional instability can distort both the frequency and amplitude leading to undesirable performance while low chemical inertness under high-intensity ultrasonication will reduce the lifespan of the sonotrode apart from contaminating the liquid. The direct approach is preferred for ultrasonication of low melting point metals such as Mg and Al. The indirect approach is useful for ultrasonicating high melting point or reactive liquids. In the chemical processing industry, indirect ultrasonication has long been used to accelerate chemical reactions, where hundreds of ultrasonic transducers are often mounted onto the outside walls of a vessel to promote intense irradiation or vibration.

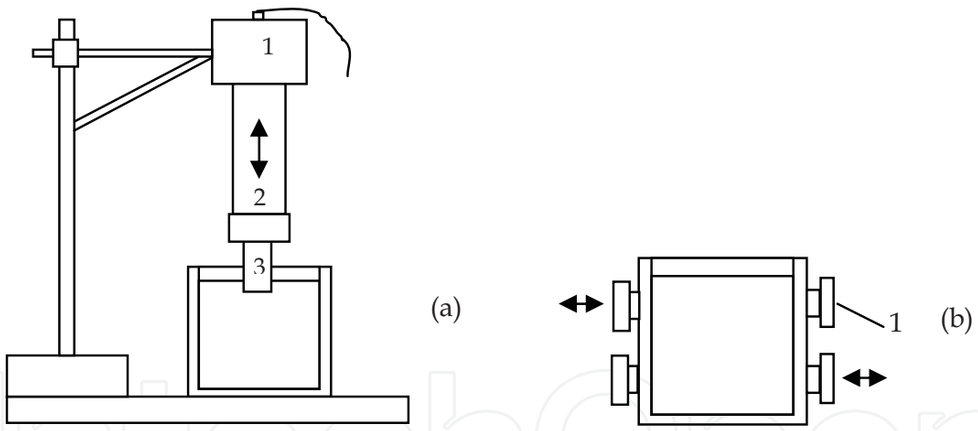


Fig. 1. (a) Direct ultrasonication: 1. ultrasonic transducer; 2. waveguide which amplifies the signal; 3. sonotrode or radiator. (b) Indirect ultrasonication: 1. transducer. Arrows denote the vibration directions, typically at a frequency of 20 kHz (Qian et al., 2009).

A commercial ultrasonic system (Fig. 1a) typically consists of a 20 kHz ultrasonic generator, a waveguide, and a sonotrode through which ultrasonic energy is transmitted to molten Mg. The intensity of ultrasonic irradiation (I) is defined by (Eskin, 1998)

$$I = \frac{1}{2}\rho c(2\pi fA)^2 \tag{1}$$

where ρ is the liquid density (ρ = 1.59 g cm^{-3} for molten Mg), c is the speed of sound, where c = 1500 m s^{-1} in molten Mg (Ramirez et al., 2008), f is the frequency, typically 20 kHz, and A is the amplitude of ultrasound. It has been established that cavitation is essential for

effective UGR and for fully developed cavitation to occur in molten light metals, the ultrasound intensity needs to be ≥ 80-100 W cm^{-2} (Eskin, 1998). The intensity can be controlled through the amplitude. For instance, I = 105, 425, 950 and 1700 W cm^{-2} corresponding to A = 7.5, 15, 22.5, and 30 μm, respectively, by Eq. (1). The amplitude of 7.5 μm is thus almost the minimum amplitude necessary for effective UGR of molten Mg. The maximum amplitude is normally < 50 μm as the resultant intensity is already significant. For instance, I = 1700 W cm^{-2} at A = 30 μm, which is ~ 20 times the threshold required for the development of full cavitation. The amplitude can be increased to 72 μm by reducing the diameter of the sonotrode to ~ 12 mm and changing the waveguide length. However, that will greatly reduce the sonotrode-melt contact interface and confine the irradiation to the vicinity of the sonotrode. In practice, it is important to ensure a maximum sonotrode-melt interface for volumetric irradiation with a well-performing amplitude (≤ 30 μm).

3. Materials and ultrasonic irradiation process

The results presented in Sections 4-8 are based on the experiments described below. Pure Mg (99.98%), binary Mg-Al and Mg-Zn alloys containing 1%, 3%, 6% and 9% of solute (all in wt.%), and three benchmark commercial Mg alloys, AZ31 (Mg-3%Al-1%Zn), AJ62 (Mg-6%Al-2%Sr), and AZ91 (Mg-9%Al-1%Zn), were irradiated during solidification. Pure Mg and binary alloys were irradiated at the maximum amplitude 30 μm while each commercial alloy was irradiated at four amplitudes, 7.5, 15, 22.5, and 30 μm.

Ingot samples of 70 mm diameter were prepared. In each experiment, 350 g of charge was melted in a clay-graphite crucible (inner diameter: 70 mm) at 730°C. After melting and alloying (for binary alloys), the crucible was withdrawn from the furnace and cooled in air. The cooling rates prior to nucleation varied between 0.76 K s^{-1} and 0.99 K s^{-1} according to the cooling curves recorded. The cooling conditions were consistent as the melt solidified in hot crucibles. This ensures that the difference in the grain size observed results mainly from the ultrasonication process and solute content.

Ultrasonic irradiation was applied through a 20 kHz commercial system (Sonic Systems Ltd, UK). Both the waveguide and sonotrode are made of Ti-6Al-4V. The sonotrode is a 25mm diameter rod with a flat radiating surface. Titanium has a negligible solubility in molten Mg (< 200 ppm at 650°C), favouring a long lifespan and minimum contamination. The melt was irradiated at 680°C by dipping the sonotrode into the crucible for 180 s. Two irradiation experiments were carried out for each condition to ensure reproducibility of results. Each irradiated ingot was sectioned longitudinally. An entire section was polished, etched, and examined. The average grain size (d) and standard deviation (σ) for each set of data reported were determined from measurements in six fields of view at 100 times. On average, about 73% of the measurements fall between $d \pm \sigma$ and 94% of the data fall between $d \pm 1.5\sigma$. The grain density, G_ρ, grains/mm^3, is calculated from the grain size assuming spherical grains.

4. Ultrasonic grain refinement of pure magnesium

The presence of an alloying element in molten Mg may alter the liquid property, for instance, its surface tension or viscosity. Accordingly, this may affect its response to ultrasonic irradiation. It is thus necessary to establish the effectiveness of ultrasonic irradiation for the grain refinement of pure Mg.

Fig. 2a shows the macro-structure of a pure Mg ingot sample solidified without ultrasonic irradiation (Ramirez & Qian, 2007). The ingot exhibited fully developed columnar grains extending to the centre, indicative of adequate purity (99.98%) of the melt. It has been shown that reducing the purity of Al from 99.99% to 99.8% will promote a columnar-to-equiaxed grain transition under conditions of forced air cooling of the melt surface in a graphite crucible (Ohno, 1987).

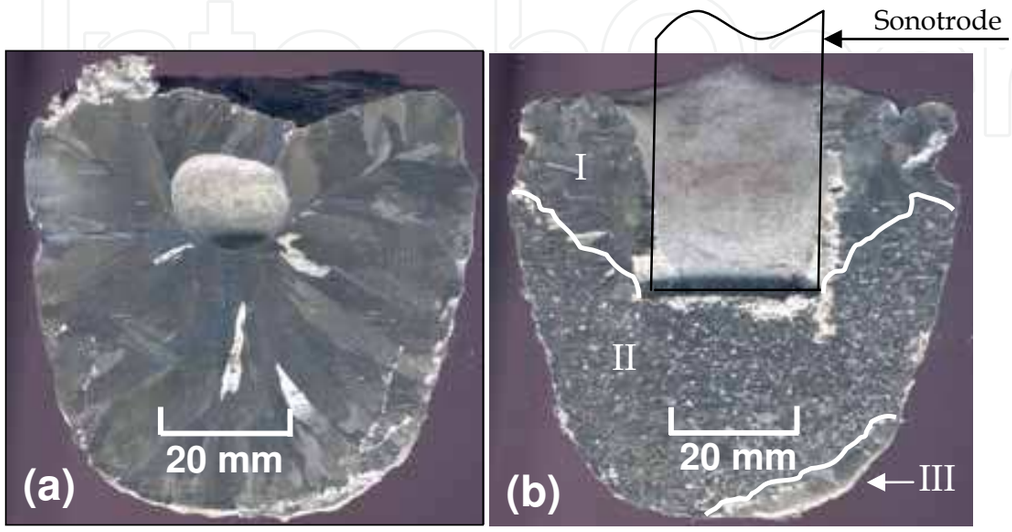


Fig. 2. Grain structures of pure magnesium: (a) without ultrasonication and (b) with ultrasonication at a nominal intensity level of 1700 W cm^{-2} (Ramirez & Qian, 2007).

Fig. 2b shows an irradiated sample, where the Ti sonotrode was dipped 35 mm into the melt. Three distinct zones are observed: a top columnar zone surrounding the sonotrode (Zone I); a nearly equiaxed zone beneath the sonotrode (Zone II); and a narrow columnar zone at the bottom (Zone III). It is interesting to note that despite the large cooling cylindrical surface of the sonotrode and the vibrations applied perpendicularly to the melt surface (Fig. 1a), UGR occurred almost exclusively below the submerged radiating face while columnar growth prevailed adjacent to the cylindrical face. The grain size is minimum (260 μm) below the radiating face and increases with ultrasound propagation distance.

Titanium has a strong growth restriction factor for Mg by the Mg-Ti phase diagram. To clarify the influence of the likely dissolution of the Ti sonotrode in the melt on the UGR, the Ti content in twelve pure Mg and AZ31 ingot samples solidified with and without ultrasonication was analysed with Inductively Coupled Plasma - Atomic Emission Spectroscopy (ICP-AES). The Fe content was also analysed as Ti is a potent iron remover. The ICP-AES analyses Ti and Fe contents down to 10 ppm each.

Table 1 lists the Ti and Fe contents obtained. There is no detectable change in the Ti content in pure Mg ingot samples after ultrasonication at 680 °C for 180 s. This is logical considering the high melting point of Ti, short ultrasonication time, and low solubility of Ti in molten Mg (~ 200 ppm at 680 °C). These results confirmed that Ti does not have any appreciable influence on the significant grain refinement observed.

The observations shown in Fig. 2b thus reflects the grain-refining capability of high-intensity ultrasonication for pure Mg, in the absence of solute, under slow cooling conditions.

Ingot sample	Before ultrasonication		After ultrasonication	
	Ti (ppm)	Fe (ppm)	Ti (ppm)	Fe (ppm)
Pure Mg	<10	51	13	35
Pure Mg	<10	30	<10	23
Pure Mg	<10	37	<10	37
AZ31	<10	31	<10	25
AZ31	<10	41	<10	11
AZ31	<10	13	<10	17

Table 1. Ti and Fe contents in pure Mg and AZ31 ingot samples ultrasonicated with an immersed 25mm diameter titanium sonotrode for 180 seconds at 680 °C (Qian et al., 2009)

5. Ultrasonic grain refinement of magnesium alloys – General observations

Ultrasonic irradiation of, either binary or multi-component commercial Mg alloys, resulted in much more potent structural refinement than that of pure Mg. Fig. 3 shows the grain structure of an ingot sample of AZ31 solidified without ultrasonication, and Figs. 4 and 5 show the refined structures of AZ31 and AZ91, respectively (Ramirez & Qian, 2007).

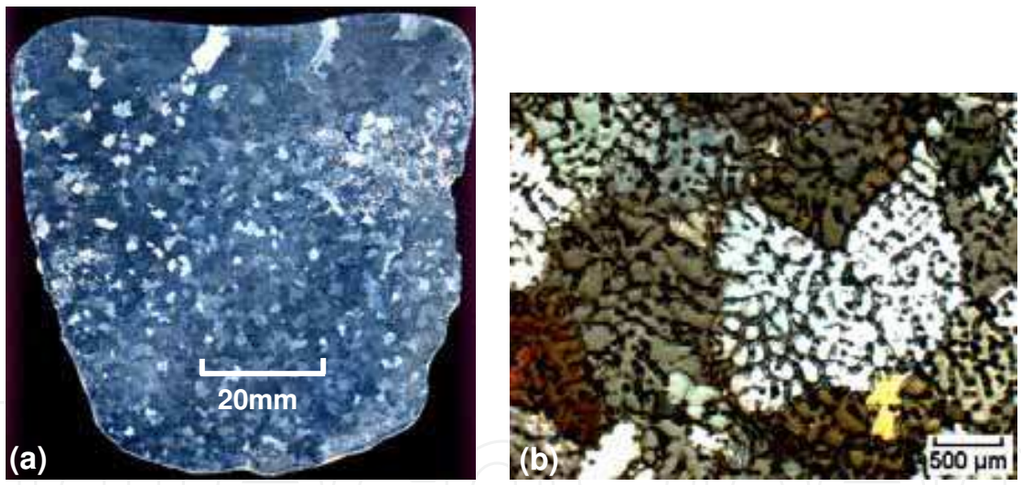


Fig. 3. Grain structures of AZ31 without ultrasonic exposure (Ramirez & Qian, 2007).

Ingot samples of AZ31 solidified without ultrasonic exposure showed coarse dendritic structure throughout the ingot, Fig. 3. The average grain size is about 2,000 µm although some dendrites have grown to ~ 4,000 µm. The macro-structure of an ingot solidified under ultrasonic irradiation and identical cooling conditions is shown in Fig. 4a. Fig. 4 b-c displays the refined equiaxed grain structures at different depths below the radiating face. The average grain size at 5 mm below the radiating face is 107 µm, demonstrating substantial UGR compared with the dendritic grains shown in Fig. 3b. The refinement decays with increasing distance from the radiating face. Far from the radiator (see Fig. 4 d, 65 mm away) rosette-like or dendritic grains are noticeable, suggesting that the local ultrasonication intensity is critical to the grain-refining process.

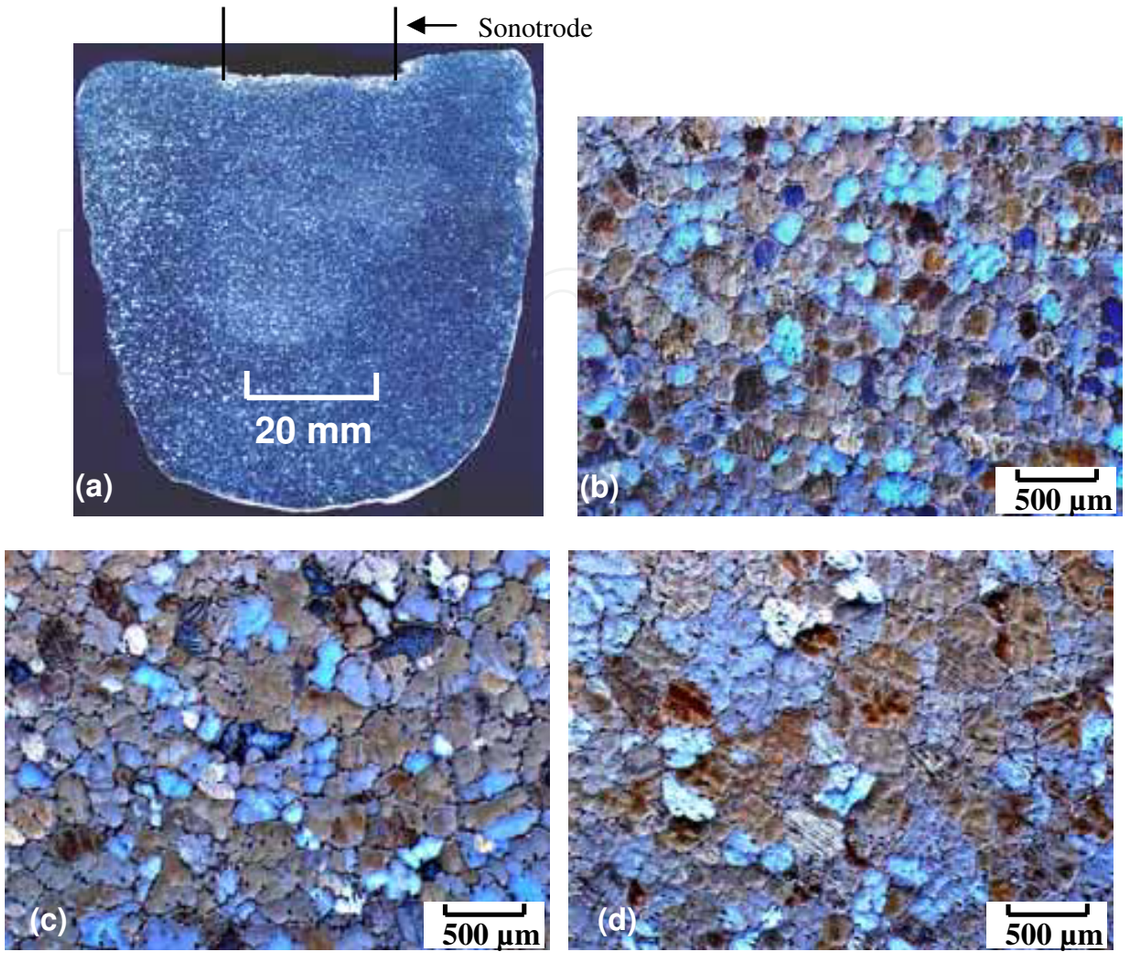


Fig. 4. Grain structures observed in an ingot sample of AZ31 solidified under ultrasonic irradiation at a nominal intensity level of 1700 W cm^{-2}. The insertion depth of the sonotrode was 1 mm. Micrographs (b), (c) and (d) were taken from 5 mm, 15 mm and 65 mm below the sonotrode radiating face, respectively (Ramirez & Qian, 2007).

Similar experiments were conducted on AZ91 in order to further assess the grain-refining potential of ultrasonic irradiation for Mg-Al based alloys. The grain structures of AZ91 ingot samples cast without ultrasonic irradiation (not shown here) are similar to those of AZ31 (Fig. 3). The average grain size is also about 2,000 µm under the slow cooling conditions used, although AZ91 was expected to have a finer grain size than AZ31 due to its high Al content.

However, ultrasonic irradiation made a substantial difference. AZ91 was found to be much more responsive to ultrasonic irradiation than both AZ31 and pure Mg. The attendant grain size is much finer and the overall grain structure is more uniform and equiaxed (Fig. 5) than the grain structures shown in Fig. 4 for AZ31. Ultrasonic irradiation of AJ62 resulted in grain refinement between AZ31 and AZ91. High-intensity ultrasonic irradiation is clearly more effective than carbon inoculation for Mg-Al based alloys; its grain-refining potency is close to that of Zr for Al-free magnesium alloys in terms of the attendant grain sizes (Ramirez et al., 2008).



Fig. 5. Grain structures of an AZ91 ingot sample solidified under ultrasonic irradiation at a nominal intensity level of 1700 W cm^{-2}. The insertion depth of the sonotrode was ~ 20 mm. Micrographs (b), (c) and (d) were taken from 5 mm, 15 mm and 45 mm below the sonotrode radiating face, respectively (Ramirez & Qian, 2007).

From pure Mg to AZ31, AJ62 and AZ91, there is a consistent indication that alloy chemistry affects the UGR of Mg alloys. A detailed assessment of the effect of solute on the UGR of Mg alloys will be presented in Section 6.2, which shows that the presence of adequate solute is crucial to attaining excellent UGR of Mg alloys.

6. Ultrasonic grain refinement of magnesium alloys – Detailed analyses

6.1 Grain size distribution

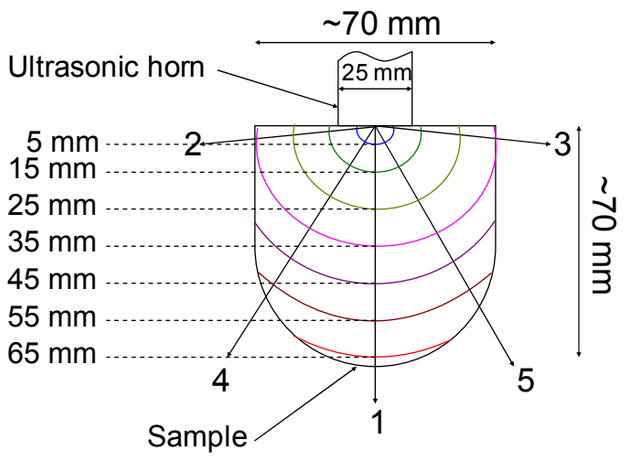
A detailed analysis of the grain size distribution along five different directions of grain-refined ingot samples of AZ31, shown schematically in Fig. 6a, was carried out. The results are summarised in Fig. 6b (1 mm insertion depth of the sonotrode) and Fig. 6c (20-25 mm insertion depth). Very similar grain size distribution patterns were observed.

A number of features can be seen from the grain size distribution shown in Fig. 6.

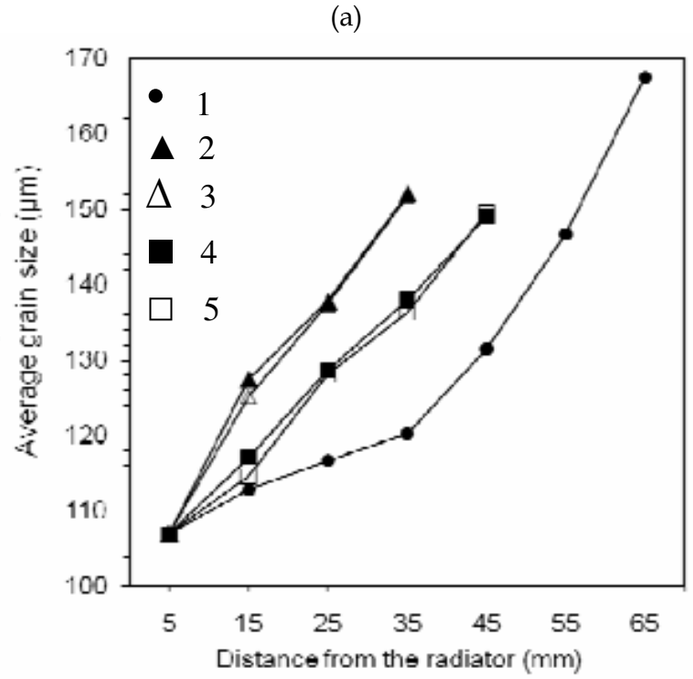
i. The grain size is the finest immediately below the ultrasonic radiator and increases with increasing distance from the radiating face in all directions.

ii. The grain size along the direction perpendicular to the ultrasonic radiator, i.e. the principal propagation direction or Direction 1 in Fig. 6a, is finer than the grain sizes observed along other directions at the same distance from the radiator.
iii. The grain size distribution is symmetrical to the principal direction, Direction 1. As can be seen, Directions 2 and 3, and Directions 4 and 5, are symmetrical. The grain size distributions overlap along these symmetrical directions.
iv. Similar grain sizes are obtained, irrespective of the immersion depth of the sonotrode, at a given distance below the radiator.
v. Although the grain size increases with increasing distance from the radiator, the ultrasonic treatment is effective throughout the volume of the melt (some rosette-like grains are observed at ~ 65 mm away from the sonotrode).

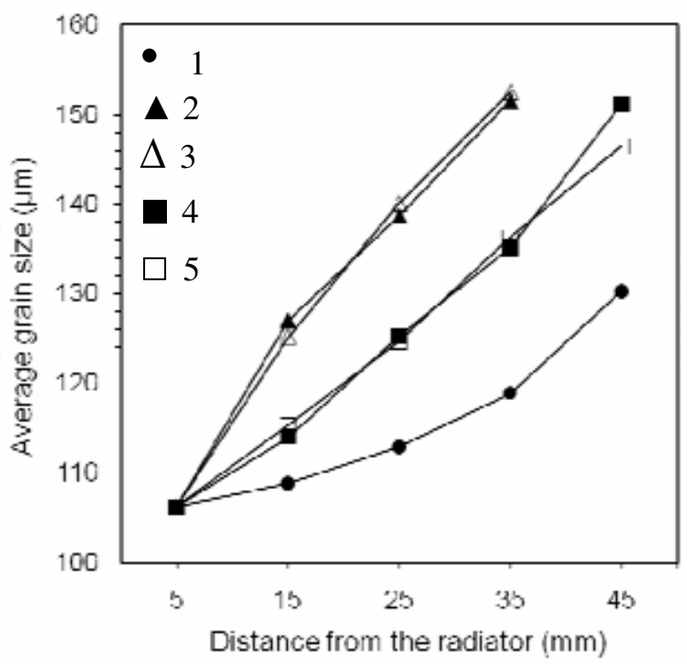
These characteristics are typical of the UGR of Mg alloys.



(a)



(b)



(c)

Fig. 6. Grain size distributions along five selected directions on polished ingot samples of AZ31 solidified under ultrasonic irradiation at a nominal intensity level of 1700 W cm^{-2}. Fig. 6a illustrates the five selected directions. The immersion depth of the sonotrode in the ingot sample for Fig. 6b is 1 mm and 20-25 mm in the ingot sample for Fig. 6c (Qian et al., 2009).

6.2 The role of solute atoms

From a solute re-distribution standpoint, liquid alloys that solidify in a high-intensity ultrasound field are subjected to high-frequency (at 20,000 Hz), small amplitude (10-50 μm) vibrations. Additionally, the collapse of bubbles (cavitation) produces violent local mixing and acoustic streaming. These dynamic conditions are expected to result in a relatively uniform distribution of solute ahead of the advancing solid-liquid interfaces and thereby diminish the growth-restriction role of solute in grain nucleation and growth.

Fig. 7 shows the average grain size versus solute content for binary Mg-Al and Mg-Zn alloys solidified without and with ultrasonic irradiation (Qian et al., 2010). Despite the substantial refinement from coarse dendritic grains to fully equiaxed fine grains, it is intriguing to note that the dependence of grain size on solute content is similar with and without ultrasonic exposure for both groups of alloys. A more detailed analysis of the role of solute will be shown in Fig. 9 and Fig. 12.

Fig. 8 a-d shows the average grain size as a function of ultrasound power represented by the square of amplitude, A^2, according to Eq. (1), and solute content for commercial magnesium alloys, AZ31, AJ62 and AZ91 (Qian et al., 2010). Without ultrasonic irradiation, all three commercial alloys solidified to dendritic grains with an average grain size of ~ 2,000 μm (see Fig. 3) under slow cooling conditions (Ramirez et al., 2008). Substantial grain refinement was obtained of each alloy even at the minimum irradiation intensity 105 W cm^{-2} ($A^2 = 7.5^2$ μm^2). These observations support Eskin's finding that an irradiation intensity level of 80-100

W cm^{-2} is required for fully developed cavitation to occur in light alloys (Eskin, 1998). They also indicate that the ultrasonic power was transmitted effectively through the titanium sonotrode, where molten magnesium wets solid titanium well (Kondoh et al., 2010).
The following observations can be made from Fig. 8 a-d.

- The average grain size decreases with increasing ultrasonic irradiation intensity but the reduction mainly occurs from 7.5^2 μm^2 to 22.5^2 μm^2; the benefits of further increasing the irradiation intensity from 22.5^2 μm^2 to 30^2 μm^2 are small.
- Increasing solute content from AZ31 to AJ62 or AZ91 consistently outweighed increasing irradiation intensity from 7.5^2 μm^2 (I_{min}) to 30^2 μm^2 (I_{max}), which represents an increase by *15 times*, i.e., (30/7.5)^2-1, at all depths. An example is illustrated in Fig. 8a, where the shorter arrowed dashed line depicts the effectiveness of increasing irradiation intensity from I_{min} to I_{max} while the longer arrowed dashed line depicts that of increasing solute content from AZ31 to AJ62 at the minimum irradiation intensity I_{min} (7.5^2 μm^2).

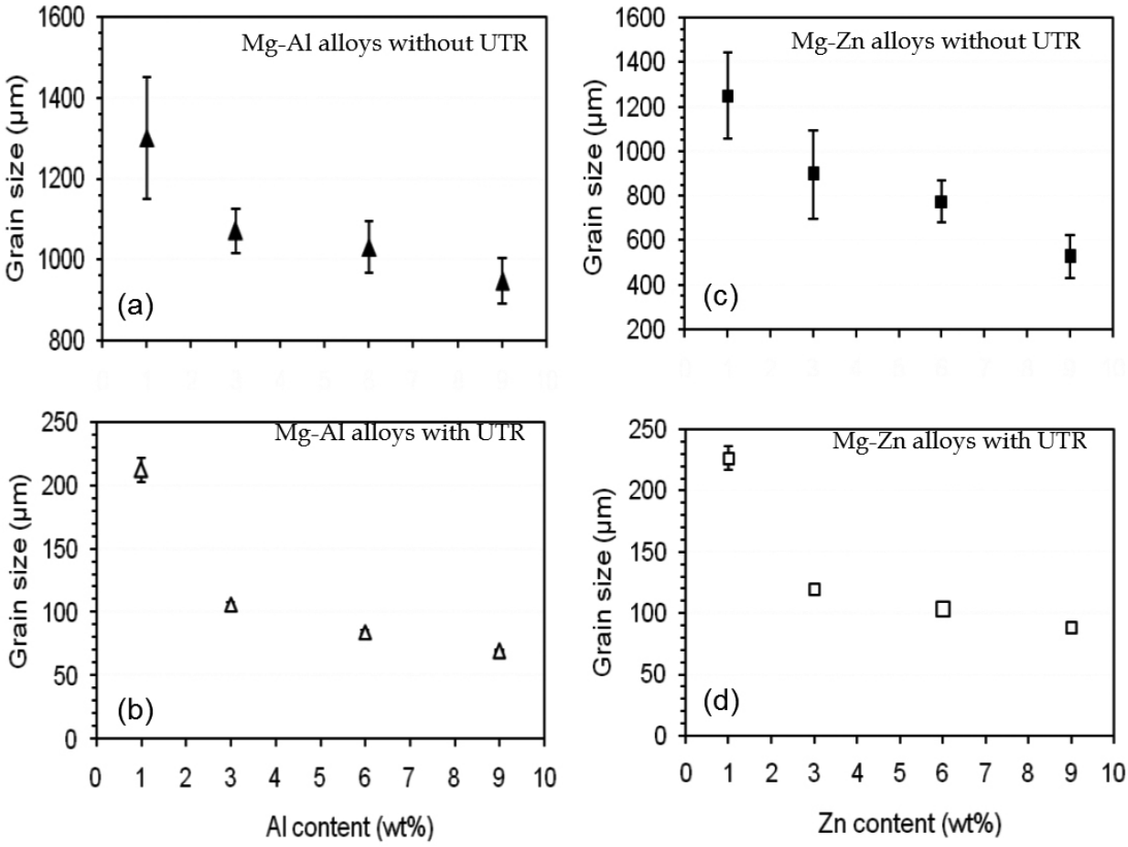


Fig. 7. Average grain size versus solute content for binary alloys without and with ultrasonication at I = 1700 W cm^{-2}. The grain size was measured at 15 mm below the radiating face. UTR: ultrasonic irradiation (Qian et al., 2010)

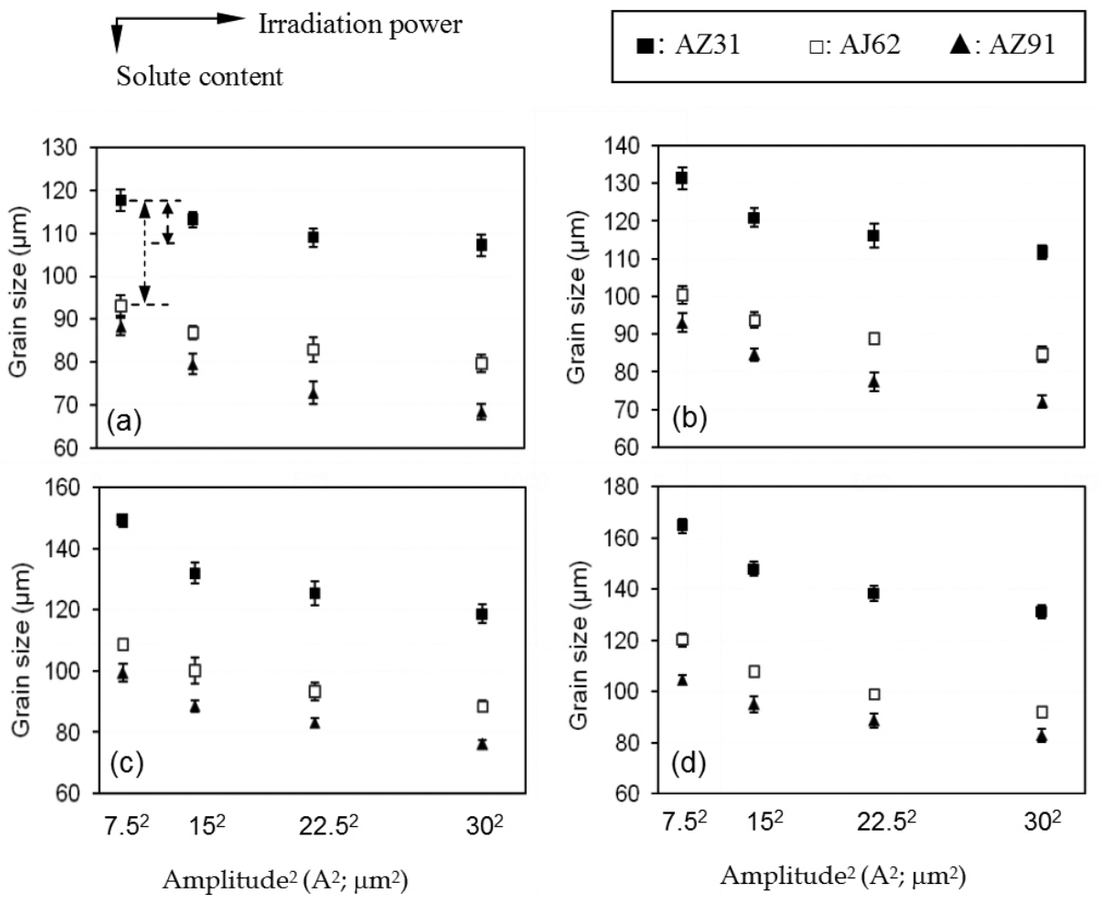


Fig. 8. Average grain size at different depths below the radiating face versus ultrasonication intensity ($I \propto A^2$) for AZ31, AJ62 and AZ91: (a) 5 mm; (b) 15 mm; (c) 30 mm; and (d) 45 mm (Qian et al., 2010)

- The *proportional* difference in the grain size between each of the alloys, for example, AZ31 and AZ91 where $d_{AZ91} \approx 0.64 d_{AZ31}$, remains approximately constant at all depths, irrespective of irradiation intensity in the range from 7.5^2 μm² to 30^2 μm². This suggests that there is little interaction between the solute content and ultrasonic irradiation intensity beyond the threshold level (7.5^2 μm²) for cavitation.
- The minimum grain size of AZ31 attained at I_{max} = 1700 W cm^{-2} (30^2 μm²) is still much greater than the grain size of AJ62 attained at I_{min} = 105 W cm^{-2} (7.5^2 μm²), although the difference in the irradiation intensity is $I_{max}/I_{min} \approx 16$ times. In contrast, the difference in the solute (Al) content between AZ31 and AJ62 is only from 3% to 6%. This further indicates that solute plays a far more important role in determining the achievable minimum grain size than the irradiation intensity.

An alternative way of evaluating the effect of solute on UGR is by examining the grain density, G_ρ, which is more closely linked to the nucleation rate. Table 2 lists the grain density calculated from the average grain size by assuming spherical grains. The grain density in each alloy that solidified in the hot crucible without ultrasonic irradiation is negligible (< 5 grains/mm³) and therefore not listed in Table 2.

Solute content (wt.%)	Mg-Zn alloys Grain density (grains mm^{-3})	Mg-Al alloys Grain density (grains mm^{-3})	Commercial alloys Grain density (grains mm^{-3})
0	64	64	64
1	165	205	
3	1116	1599	1559 (AZ31: 3%Al)
6	1722	3245	3744 (AJ62: 6%Al)
9	2793	5640	5788 (AZ91: 9%Al)

Table 2. Grain densities of binary Mg-Zn and Mg-Al and commercial AZ31, AJ62 and AZ91 alloys calculated from the grain size at 15 mm below the sonotrode-melt interface, irradiated at $A^2 = 30^2$ μm² (Qian et al., 2010)

The grain density increases enormously with increasing solute content under the same irradiation conditions. For instance, it increased from 205 to 5640 grains/mm³ with increasing Al content from 1% to 9%. In fact, the grain density and solute content exhibit an unexpected linear relationship for each alloy system. Fig. 9 shows the results (Qian et al., 2010). Also indicated is the grain density of pure Mg irradiated under similar conditions.
Fig. 9 reveals that there must be adequate solute present in each alloy for significant grain refinement ($G_\rho \geq 2000$ grains/mm³ or $d \leq 100$ μm) to occur by ultrasonic irradiation. Under the slow cooling conditions used, it requires a minimum of ~ 6.5% Zn for binary Mg-Zn alloys and a minimum of ~ 3.5% Al for binary Mg-Al alloys. Commercial grade AZ31 is just about all right as it contains 3%Al and 1%Zn. This benchmark wrought Mg alloy can thus be effectively refined by ultrasonic irradiation, although having a higher solute content will further enhance the refinement as shown by AJ62 and AZ91 in the same plot.

6.3 The role of wall crystals

Wall crystals can play an important role in metal solidification as demonstrated by Ohno (Ohno, 1987). The melt surface vibration experiments performed by Ohno (Ohno, 1987; Qian et al., 2009) are essentially similar to the application of ultrasonic vibration to the melt surface through a bar-type titanium sonotrode, which traverses perpendicularly to the melt surface as illustrated in Fig. 1a. Apart from transmitting ultrasonic energy, the titanium sonotrode, whose diameter varies from a few millimeters to over 100 mm depending on the volume of the liquid, also acts as a big chill to absorb and conduct heat away from the melt due to the substantial difference in the melting point of Ti (1660°C) and the melt temperature (≤ 800°C for light metals). Accordingly, it is anticipated that the immersed surface of the Ti sonotrode will provide a primary cold surface for the formation of wall crystals. Also, it would seem reasonable to further assume that many such wall crystals will separate from the surface of the Ti sonotrode due to the high frequency (20 kHz) transverse movements of the rod and consequently play an important role in the UGR of light metals. Hence understanding the role of wall crystals in ultrasonic refinement will help understand the mechanism by which ultrasonication refines the microstructure and facilitate designing a more efficient ultrasonic refining system.

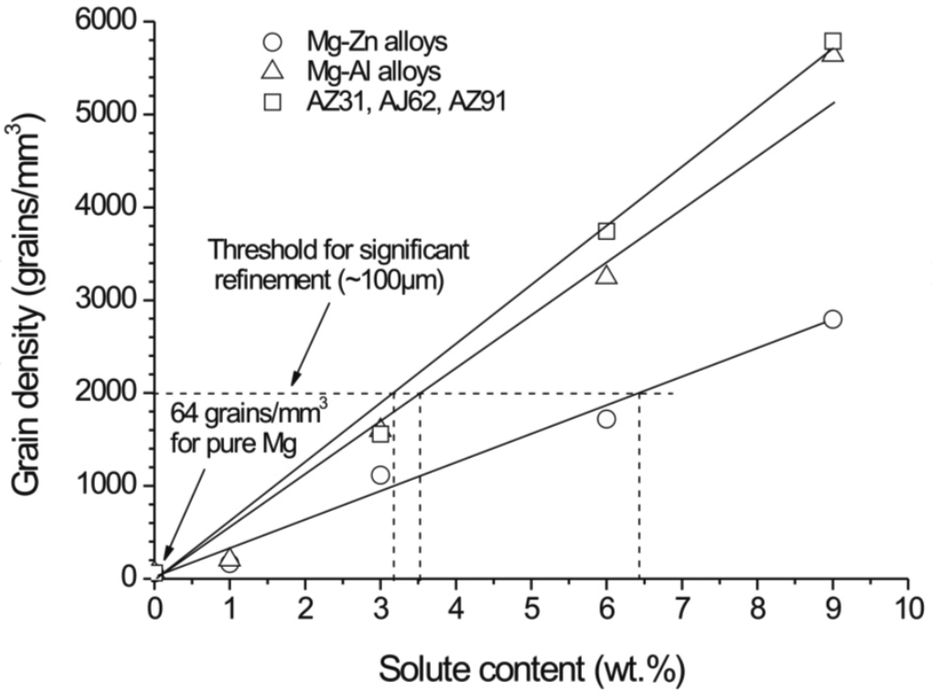


Fig. 9. Grain density versus solute content for magnesium alloys irradiated at 1700 W cm^{-2} or $A^2 = 30^2$ μm^2 (Qian et al., 2010)

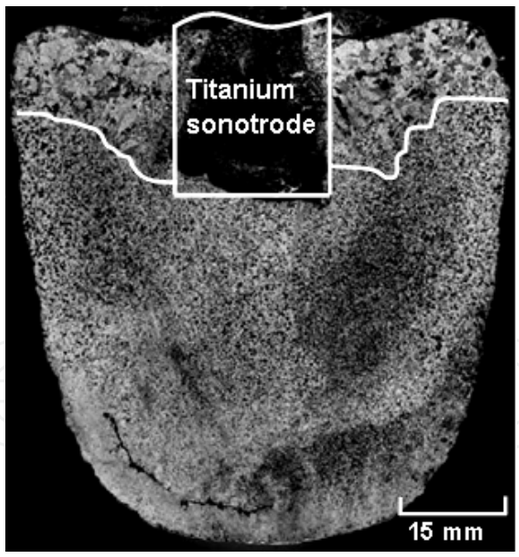


Fig. 10. Ultrasonic refinement of AZ31 at a nominal intensity level of 1700 W cm^{-2}.

Fig. 2b shows that ultrasonic grain refinement of pure Mg occurs only below the radiating face; little refinement was observed adjacent to the cylindrical face of the sonotrode immersed in the melt. To clarify if the observation occurs only to pure Mg, similar immersion experiments were conducted on AZ31. Fig. 10 shows the macro-structure of an AZ31 ingot sample solidified under ultrasonic irradiation (Qian et al., 2009), where the titanium sonotrode was submerged about 25 mm into the melt. Similarly, ultrasonic grain

refinement was observed almost exclusively below the radiating face. The borderlines that distinguish the refined and unrefined regions are indicated in Fig. 10.

Considering that the colder sonotrode surface provides an effective surface for nucleation due to its chill effect and transverse motion, the occurrence of columnar growth around the cylindrical sonotrode face for both pure Mg (Fig. 2b) and AZ31 (Fig. 10) indicates that the anticipated formation and detachment mechanism was ineffective. More interestingly, as shown by Fig. 6b and c, the actual grain sizes and grain size distribution patterns are almost independent of the insertion depth of the ultrasonic radiator. This demonstrates negligible influence of the chill surface (source of wall crystals) on the observed refinement.

The formation of columnar zones around the cylindrical face of the immersed sonotrode can be explained as follows. The efficient chill effect of the sonotrode produces a large thermal gradient around the cylindrical face and promotes directional growth of nucleated crystals perpendicular to the sonotrode. However, the lack of convection in this region will deter the detachment and melting of the crystals at their base thereby favouring coarse columnar growth. In addition, the small amplitude of vibration (30 μm) of the sonotrode is probably inadequate to mechanically shear off the wall crystals from the sonotrode surface before columnar growth occurs. According to Ohno (Ohno, 1987), once a solid shell of columnar grains forms on a cold contact with high cooling capacity, it will be difficult for the columnar crystals to separate even though movement of molten metal still exists. On the other hand, it is plausible that some wall crystals have formed and separated from both the surfaces of the sonotrode and the crucible walls, but the total population is negligible compared to the number of the crystal nuclei created by cavitation-enhanced nucleation. Under the experimental conditions, the minimum grain size of a pure Mg ingot sample is about 2,000 μm (see Fig. 2a, edge of the ingot at the bottom). This roughly corresponds to a grain density of ~ 0.24 mm^{-3}. In contrast, the grain density attained in pure Mg immediately below the radiating face is ~ 100 mm^{-3} (average grain size: 260 μm), which is about 400 times the grain density originating from the wall crystals. The wall crystal effect is thus fairly negligible under the experimental conditions even if the mechanism has been operative during ultrasonication.

7. Ultrasonic attenuation in molten magnesium alloys

Similar to propagation in water, when an ultrasonic wave travels through a liquid metal, its amplitude (A) and intensity (I) attenuate with distance. Consequently, ultrasonication will be confined to a limited volume of the liquid beyond which the intensity is insufficient to induce desired structural refinement. It is thus necessary to understand the process both for effective UGR and the design of a performing ultrasonic system.

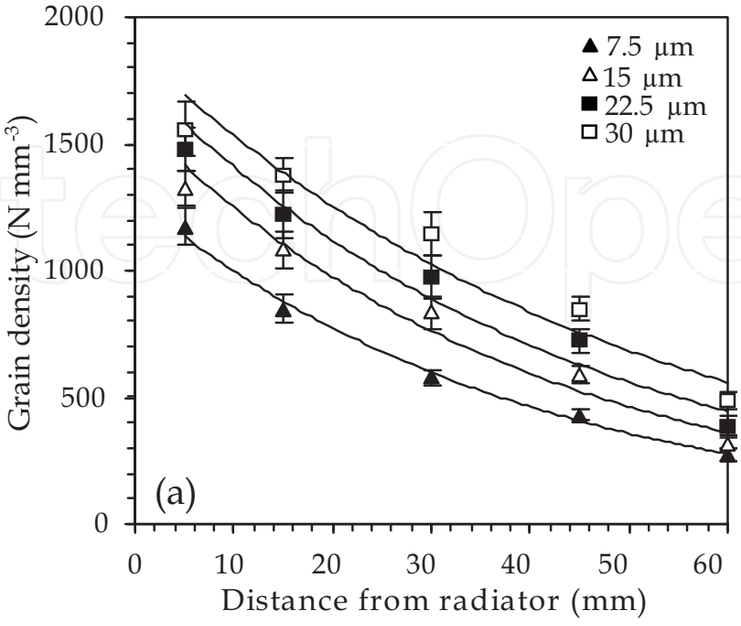
The Stokes-Kirchhoff relation allows prediction of the attenuation coefficient α of an ultrasonic wave in a liquid by the addition of a viscous component α_v and a thermal component α_T in the form (Sahu, 1984; Awasthi & Murthy, 1985; Kuttruff, 1991)

$$\alpha = \alpha_v + \alpha_T = \frac{2\pi^2}{\rho c^3}\left[\frac{4}{3}\eta + \lambda_T\left(\frac{1}{c_v} - \frac{1}{c_p}\right)\right] f^2 \tag{2}$$

In Eq. (2), ρ is the density (kg m^{-3}), c is the velocity of ultrasound (m s^{-1}) in the liquid, η is the viscosity (N s m^{-2}), λ_T is the thermal conductivity (W m^{-1} K^{-1}), f is the ultrasonic frequency (Hz), and c_v and c_p are specific heats at constant volume and pressure, respectively (J kg^{-1} K^{-1}). However, it has been found that the predictions given by Eq. (2) for low melting point metals (< 350°C) are much smaller than the experimental measurements (Sahu, 1984; Awasthi & Murthy, 1985). For molten Mg (T_m = 650°C), ρ = 1590 kg m^{-3}, c =1500 m s^{-1} (Ramirez et al., 2008), η = 1.25 mN s m^{-2}, λ_T = 78 W m^{-1} K^{-1}, and c_p = 1.36 J g^{-1} K^{-1} (Brandes, and Brook, 1992), where for most liquids, c_p/c_v = 1.0-1.1. Eq. (2) gives α = (2.45-10.89)×10^{-6} m^{-1} for molten Mg with respect to f = 20 kHz. The predicted value of α is too small and contradicts experimental observations.

A practical approach has recently been proposed to assess the ultrasonic attenuation in light metals and alloys (Qian & Ramirez, 2009). For Mg alloys, the attenuation can be assessed by the variations of the grain density with propagation distance in relation to the ultrasonication intensity applied (Qian & Ramirez, 2009). Fig. 11 (a) to (c) depicts the variations of the grain density (G_ρ) for AZ31, AJ62 and AZ91 along the principal propagation direction (Direction 1 in Fig. 6) with respect to different ultrasonic amplitudes. A detailed analysis revealed that the reduction in G_ρ with propagation distance is best described, in an exponential form of $G_\rho = G_\rho(0)e^{-\alpha x}$, where $G_\rho(0)$ is the grain density at the radiating face in the solidified sample and α is attenuation coefficient. The exponential curves of best fit are shown in Fig. 11 for each condition.

Table 3 summarizes the characteristic attenuation coefficients (α) for each alloy determined from Fig. 11. As expected, α exhibited dependence on alloy composition, where a significant decrease in the value of α was observed with increasing solute content from 3%Al to 6%Al but a further increase of the solute content to 9%Al resulted in only a marginal decline. A low attenuation coefficient implies that the molten alloy can be readily ultrasonicated. So, both AJ62 and AZ91 are more ultrasonicatable than AZ31. Consequently,



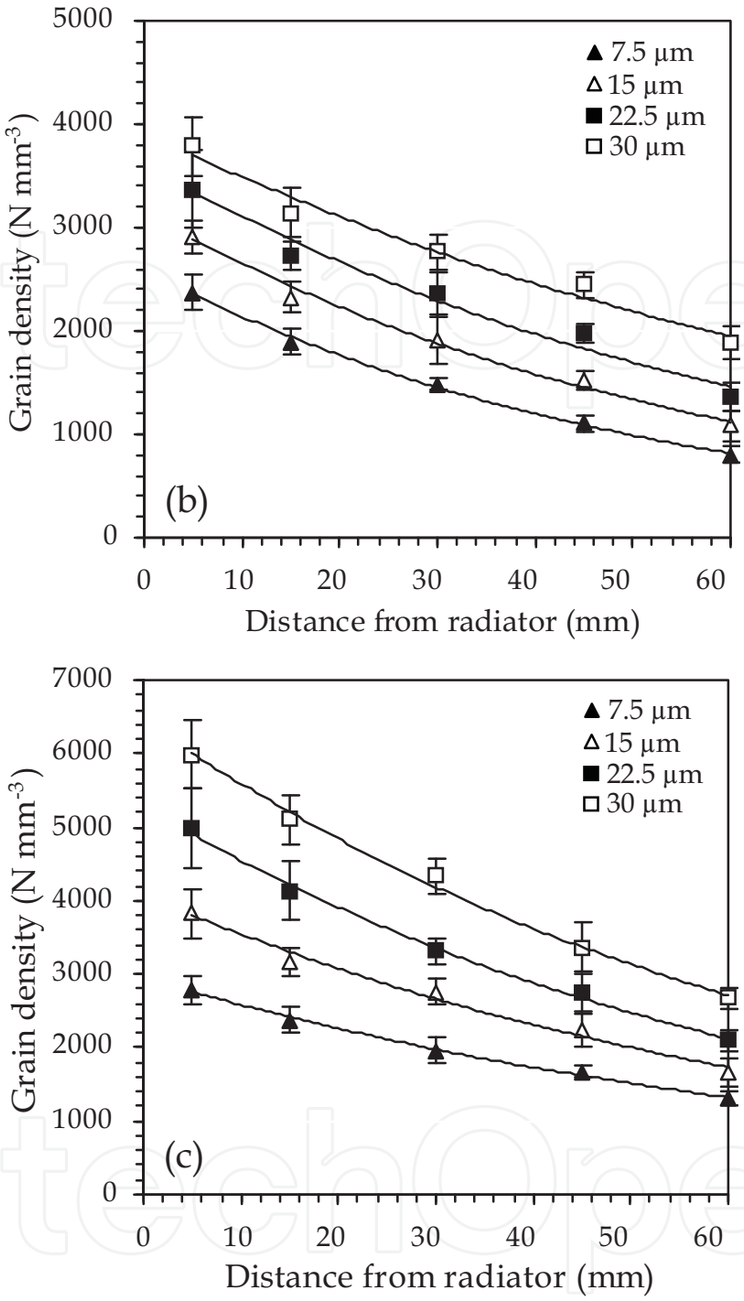


Fig. 11. Grain density versus propagation distance along the principal propagation direction with respect to different amplitudes for (a) AZ31, (b) AJ62 and (c) AZ91.

to exploit the structural refining potential of ultrasonic irradiation, it is important to develop low attenuation coefficient alloys. Alloy chemistry plays a critical part in this regard. This also provides a means of controlling the attenuation behaviour in molten Mg alloys. The characteristic attenuation coefficient determined for AZ31 was validated by comparing predictions with experimental observations from ultrasonicating 140 mm diameter ingot samples, and also with Eskin's work (Qian & Ramirez, 2009).

Liquid alloy (wt.%)	Attenuation coefficient α (mm^{-1})	Standard deviation (mm^{-1})
Mg-3Al-1Zn (AZ31)	0.0234	0.002394
Mg-6Al-2Sr (AJ62)	0.015825	0.003241
Mg-9Al-1Zn (AZ91)	0.01435	0.000742

Table 3. Characteristic ultrasonic attenuation coefficients in liquid Mg alloys (Qian & Ramirez, 2009).

Attenuation is a concern for the structural refinement on a large scale. Alloy design can effectively mitigate the problem according to the attenuation coefficient results listed in Table 3.

8. Mechanism of ultrasonic grain refinement

The influence of ultrasonic irradiation on structural refinement is based on the physical phenomena arising out of high-intensity ultrasound propagation through liquid. Several mechanisms have been proposed and the major ones may be summarised as cavitation-induced dendrite fragmentation, cavitation-enhanced heterogeneous nucleation, and vibration-stimulated separation of wall crystals.

The cavitation-induced dendrite fragmentation hypothesis assumes that the shock waves generated from the collapse of bubbles lead to fragmentation of dendrites, which are redistributed through acoustic streaming, thereby increasing the number of crystals (Flemings, 1974). The cavitation-enhanced heterogeneous nucleation theory is further explained by three different mechanisms. The first is based on the pressure pulse–melting point (T_m) mechanism (Hunt & Jackson, 1966), where the pressure pulse arising from the collapse of bubbles alters T_m according to the Clapeyron equation. An increase in T_m is equivalent to increasing the undercooling so that an enhanced nucleation event is expected. It has been estimated that at the collapse point of a gas-filled bubble in water the pressure produced is of the order of between 1000 and 4000 atm (Knapp et al., 1970). The attenuation of the maximum-pressure intensity is proportional to $1/r$, where r is the distance from the collapse centre. At a distance of $r/R = 2$, where R is the bubble radius, the pressure is estimated to be of the order of 200 to 1000 atm (Knapp et al., 1970). Using the Clapeyron equation and the typical parameters for magnesium summarised in (Qian, 2006), we found that the increase in the melting point of magnesium or undercooling by a pressure pulse of one atmosphere is about 0.00647 K. For nickel it is about 0.0027 K (Chalmers, 1964). For a given pressure pulse of 1000 atmospheres, that is equivalent to introducing an "additional undercooled zone" with $\Delta T = 6.47$ K. This will suffice to trigger nucleation on most substrates present in the undercooled zone. The second is based on cavitation-enhanced wetting (Eskin, 1998), which assumes that cavities and cracks on the substrate surfaces and insoluble non-metallic inclusions that either pre-exist in the melt or form on cooling during solidification, can be wetted by the melt under the pressure pulse from the collapse of the bubbles. Consequently, this enables these substrates to act as effective nucleation sites (Eskin, 1998). The third mechanism assumes that rapid adiabatic expansion of gas inside the bubbles created during cavitation undercools the liquid at the bubble-liquid interfaces

resulting in nucleation on the bubble surfaces (Hunt J. D. & Jackson, 1966; Jian et al., 2005). Collapsing of these bubbles will distribute the nuclei into the surrounding liquid producing a significant number of nuclei in the liquid.

The wall crystal hypothesis was proposed by Ohno (Ohno, 1987). It was suggested that vibration refines the microstructure by two means. First, since a molten metal is constantly covered with oxide films, the contact of the molten metal with the mould walls or a cold contact surface can hardly be uniform under usual conditions. Vibration could disrupt the covering oxide films promoting wetting of the mould walls by the molten metal. This enhances the nucleation of the wall crystals on the mould or cold contact surfaces. The second aspect is that vibration promotes the separation of the crystals of a thin necked shape from the mould walls due to the local shaking and/or shearing effects caused by vibration. These two effects combine together to produce a substantial number of crystal nuclei responsible for the refinement. Recent work has clarified that the wall crystal mechanism does not play any appreciable role in the UGR of Mg alloys (Qian et al., 2009).

The role of solute was not considered in the mechanisms proposed previously. It is clear from Figs. 8 and 9 that solute plays a decisive role in the UGR of Mg alloys. This generally goes against the perception that solute homogenisation could be enhanced under ultrasonic induced fluid flow reducing the growth restriction effect. Solidification under ultrasonic irradiation is known to be more dynamic compared with solidification under quiescent conditions (Chalmers, 1964). An immediate question that follows is: what are the roles that ultrasonic irradiation and solute each play in the structural refinement? A new mechanism is proposed below for ultrasonic grain refinement of Mg alloys.

First, high-intensity ultrasonic irradiation plays a key role in producing the first batch of nuclei or crystallites in the effectively irradiated volume near the sonotrode by enhanced nucleation, due to enhanced wetting of the insoluble nucleating particles and/or the pressure effect on melting point. These crystals are then continuously dispersed into other parts of the melt as nuclei or crystallites by the dynamic effects generated by ultrasonic irradiation. In a direct ultrasonication process, the sonotrode was immersed below the melt surface in the middle of the melt. Crystals are thus dispersed from the middle of the melt towards the crucible walls. Without ultrasonic irradiation the chance of creating a large number of initial nuclei and having them dispersed in the bulk melt at the same time are generally very limited. This is because nuclei originating from either the mould wall reaching and then surviving in the bulk superheated melt would have been very small in number. In contrast, high-intensity ultrasonication directly creates nuclei in the irradiated bulk melt. Therefore it fundamentally changes the sequence of solidification compared to conventional ingot solidification. Second, the high-frequency (20,000 Hz) and small amplitude (7.5-30 μm) vibrations in conjunction with the strong cavitation effects help dissipate heat from the effectively irradiated volume so that many of the crystals formed in the melt have a better chance to survive. This differs from the low survival rate of wall crystals in conventional ingot solidification. On the other hand, new crystals are being continuously generated by ultrasonic irradiation to serve as fresh nuclei or growing fronts. Ultrasonic irradiation thus acts as a continuous crystal generator to inoculate the solidifying melt with a large number of *initial crystallites*. For instance, in the case of AZ91, the number of grains formed under ultrasonic irradiation is in the order of 5788/mm^3 (Table 2) compared to a negligible grain density of 0.24 (~ 2,000 μm grain size) under the same slow cooling conditions.

Once the initial crystallites are generated in an alloy melt by ultrasonic irradiation, growth of each crystal will lead to solute enrichment ahead of each growing front. The attendant constitutional supercooling (ΔT_{cs}) will further induce nucleation on nearby most potent available nucleants when ΔT_{cs} is greater than the undercooling required for nucleation (ΔT_n) (Qian et al., 2010b). The concept has been formulated on a rigorous basis to predict grain formation in Al, Mg and Ti alloys solidified under various conditions (Qian et al., 2010b). It confirms the existence of a fundamental linear relationship between the average grain size d and the growth restriction factor $Q = m_l \cdot c_0 \cdot (k-1)$, where c_0 is the solute concentration, m_l the slope of the liquidus, and k the solute partition coefficient. The linear relationship assumes

$$d = a + D \cdot \Delta T_n / (v \cdot Q) \tag{3}$$

where a is a constant, D is diffusion coefficient and v is growth velocity. A detailed account has been given of the historical evolution of this linear relationship in the work referenced (Qian et al., 2010b).

Fig. 12 plots the average grain size obtained at 15 mm (Fig. 12a) and 30 mm (Fig. 12b) below the radiating face for AZ31, AJ62 and AZ91 versus $1/Q$ with respect to each intensity level applied. An excellent linear relationship was observed. The average grain size versus $1/Q$ at other depths below the radiating face showed similar linear relationships.

It is clear from Fig. 9 that the presence of solute considerably enhances grain density. In fact, only a very low number of crystals in the order of 64/mm^3 (Table 2) would survive to produce the final grain structure if no solute were present. This suggests that the development of a constitutionally undercooled region around each initial crystallite may be critical in ensuring the survival of the ultrasonically produced crystallites. This explains the strong dependence of grain size on solute composition shown in Fig. 12.

It should be noted that the formation of a sufficient number of initial crystallites or presence of numerous nucleating particles is essential to the ultrasonic grain-refining process, particularly for commercial alloys in which native nucleants are often poisoned by impurities (Cao et al., 2005). For example, without ultrasonication, little effect of solute was observed in the three commercial alloys when solidified under the same slow cooling conditions (Ramirez et al., 2008), where they all showed a similar coarse grain structure of d ≈ 2,000 μm. This is because there were few active nucleants operating in these alloys to initiate the growth-restriction effect of solute. This was confirmed by the negligible grain density of 0.24 grains/mm^3 (d ≈ 2,000 μm) observed in each solidified alloy ingot (Ramirez et al., 2008). Accordingly, it supports the idea that ultrasonic irradiation is a nucleation facilitator or crystallite generator. However, the degree of survival of these crystallites is determined by the solute content of the alloy.

In a continuous ultrasonic irradiation process, as the effect of solute develops ahead of the growing crystals, new crystallites will be continuously generated and dispersed into other parts of the melt. This development will gradually extend into the entire melt where the growth restriction effect of solute similarly applies. So, once the irradiation intensity is above the cavitation threshold, which means that the irradiation applied is able to generate a sufficient number of initial crystals, the subsequent development of the solidification process will be mainly determined by the growth restriction role of solute. Ultrasonic grain

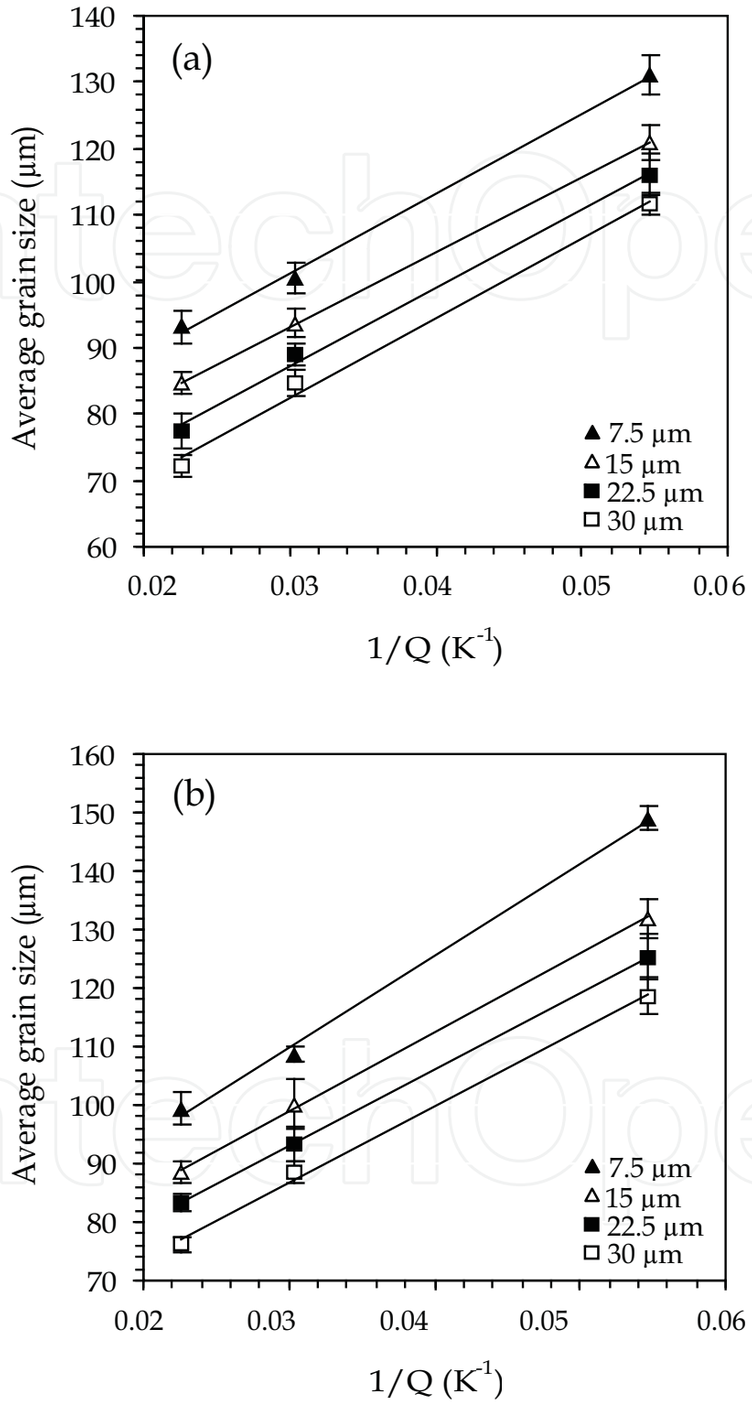


Fig. 12. Average grain size measured at 15 mm (a) and 30 mm (b) below the radiating face versus 1/*Q* for AZ31, AJ62 and AZ91 (Qian & Ramirez, 2009).

refinement of Mg alloys thus arises from the combined effects of ultrasonic irradiation and solute. Both effects are important to ensure significant refinement. There is little need to pursue extremely high irradiation intensity levels. Instead, it appears to be more important to exploit the effect of solute through alloy design by using an appropriate level of irradiation intensity such as $A^2 = 15^2$ μm² or 22.5^2 μm². Finally, it should be noted that solute affects the physical properties of a liquid alloy including the surface tension and viscosity, which may affect cavitation. Any detailed assessment of such influences will facilitate the selection of solutes for ultrasonic grain refinement.

The proposed mechanism explains most observations made from this study. Given the importance of solute under ultrasonic irradiation in ensuring a fine grain structure, the proposed mechanism is expected to apply to ultrasonic irradiation of all alloy systems that are made up of growth restricting elements. Regarding the inference that ultrasonic irradiation showed little influence on solute redistribution even at the irradiation intensity level of 1700 W cm^{-2}, our proposal is that the dynamic effects from ultrasonic irradiation may only affect the solute boundary layer by a limited amount over a short timescale; they do not largely interfere with the evolution of an appreciable constitutional undercooling zone. This needs to be examined in greater detail in the future.

9. Summary and conclusions

- Ultrasonic irradiation of magnesium alloys at intensity levels above the melt cavitation threshold leads to significant structural refinement (≥ 2,000 grains/mm^3 or ≤ 100 μm grain size) *only in the presence of adequate solute*. Without solute, high-intensity (1700 W cm^{-2}) ultrasonic irradiation of pure magnesium results in grain densities only in the order of 64 grains/mm^3 while in the presence of 9%Al the grain density increases to 5640 grains/ mm^3 under the same irradiation conditions. Grain refinement of magnesium alloys by ultrasonic irradiation shows strong dependence on solute content.
- For significant grain refinement to occur by ultrasonic irradiation, the minimum solute required is ~ 6.5%Zn for binary Mg-Zn alloys and ~ 3.5%Al for binary Mg-Al alloys under cooling conditions of 0.76 - 0.99 K s^{-1}. Commercial grade AZ31 is just about all right as it contains 3%Al and 1%Zn.
- Increasing solute content at an appropriate irradiation intensity level (i.e. above the cavitation threshold) is more effective for grain refinement than substantially increasing irradiation intensity. The difference in the grain size between two magnesium alloys solidified under ultrasonic irradiation is mainly determined by the solute content rather than the irradiation intensity. In view of these, there is little need to pursue excessive irradiation.
- The primary role of ultrasonic irradiation is to produce the initial crystallites by enhanced nucleation in the effectively irradiated melt volume. The role of solute with a high growth-restriction factor is twofold. Firstly, the constitutionally undercooled region developed around each growing initial crystallite protects them from remelting. Growth of these crystals then generates constitutional undercooling sufficient to cause further grain nucleation in regions away from the sonotrode. Ultrasonic grain refinement of Mg alloys arises from the combined effects of solute and irradiation and both effects are important.

- The effect of ultrasonic irradiation on solute redistribution in a solidifying magnesium alloy seems rather limited even at a substantial intensity level such as 1700 W cm^{-2}. Solute plays a similar role with and without high-intensity ultrasonic irradiation.
- Ultrasonic grain refinement occurs almost exclusively below the radiating face of the sonotrode; little refinement is observed in the solidified ingot adjacent to the immersed cylindrical face of the cold titanium sonotrode, which oscillates perpendicularly to the melt surface at an amplitude of 30 μm and a frequency of 20 kHz. The insertion depth of the sonotrode in the melt has no impact on the resulting ultrasonic refinement. The formation and separation of wall crystals from the titanium sonotrode has negligible influence on the observed refinement.
- Ultrasonic grain refinement is symmetrical to the principal ultrasound propagation direction; the grain size along the principal propagation direction is the smallest at the same distance from the radiating face. The grain size increases with increasing distance from the radiating face in all directions.
- Attenuation of ultrasound intensity in molten Mg alloys can be effectively assessed according to the variations of the grain density with propagation distance. Metallographic analyses reveal that the dependence of grain density on ultrasound propagation distance obeys an exponential law with respect to different amplitudes. The attenuation of ultrasound amplitude with propagation distance can be described by the same exponential law. The characteristic attenuation coefficients in three benchmark molten magnesium alloys, AZ31 (Mg-3Al-1Zn), AJ62 (Mg-6Al-2Sr) and AZ91 (Mg-9Al-1Zn), have been determined. The coefficient is alloy dependent.
- High-intensity ultrasonic irradiation is more potent than carbon inoculation for Mg-Al based alloys; its grain-refining potency is close to that of Zr for Al-free magnesium alloys (Ramirez et al., 2008).

10. Acknowledgements

Financial support from the UK government's Engineering and Physical Sciences Research Council (EPSRC) is acknowledged. Magnesium Elektron Ltd., UK is acknowledged for both financial support and provision of experimental materials. Useful discussions with Dr A. Das of the School of Engineering, Swansea University, Singleton Park, Swansea, SA2 8PP, UK are acknowledged.

11. References

Abramov O. V. (1994). *Ultrasound in Liquid and Solid Metals*, CRC Press, ISBN 0801649307, Boca Raton, FL.

Awasthi O. N. & Murthy B. V. S. (1985). *Phys. Lett*. A, Vol. 108, 119-122, ISSN 0375-9601.

Brandes E. A. & Brook G. B. (1992). *Smithells Metals Reference Book* (7th ed.), Butterworth-Heinemann, ISBN 0408046228, Oxford.

Cao P., Qian M. & D.H. StJohn (2005). *Scripta Mater.*, Vol. 53, 841-844, ISSN 1359-6462.

Chalmers B. (1964). *Principles of Solidification*, 86-89, John Wiley, ISBN 0471143251, NY.

Emley E. F. (1966). *Principles of Magnesium Technology*, Pergamon, ISBN 0080106730, Oxford.

Eskin G. I. (1998). *Ultrasonic Treatment of Light Alloy Melts*, Gordon & Breach, ISBN 905699042X, Amsterdam.

Flemings M. C. (1974). *Solidification Processing*, 300, McGraw-Hill, ISBN 007021283X, NY.

Hunt J. D. & Jackson K. A. (1966). *J. Appl. Phys.*, Vol. 37, 254-257, ISSN 0021-8979.

Jian X., Xu H., Meek T. T. & Han Q. (2005). *Mater. Lett.*, Vol. 59, 190-193, ISSN 0167-577X.

Jian X., Meek T. T. & Han Q. (2006a). *Scripta Mater.*, Vol. 54, 893-896, ISSN 1359-6462.

Jian X., Meek T., Geer T. & Han Q. (2006b). *Magnesium Technology 2006*, pp. 103-107, ISBN 978-0-87339-620-2, San Antonio, TX, March 2006, TMS, Warrendale, PA.

Knapp R. T., Daily J. W. & Hammitt F. G. (1970). *Cavitation*, 143-145, McGraw-Hill, NY.

Kondoh K., Kawakami M., Imai H., Umeda J. & Fujii H. (2010). *Acta Mater.*, Vol. 58, 606-614, ISSN 1359-6454.

Kuttruff H. (1991). *Ultrasonics: Fundamentals and Applications*, 209, Elsevier, ISBN 1851665536, London.

Lide D. R. (2001). *CRC Handbook of Chemistry and Physics* (82nd ed.), 6-3, CRC Press, ISBN 0849304822, Boca Raton.

Liu X., Osawa Y., Takamori S. & Mukai T. (2008). *Mater. Sci. Eng. A*, Vol. 487, 120-123, ISSN 0921-5093.

Liu Q., Zhai Q., Qi F. & Zhang Y. (2007). *Mater. Lett.*, Vol. 61, 2422-2425, ISSN 0167-577X.

Ohno A. (1987). *Solidification: The Separation Theory and Its Practical Applications*, Springer, ISBN 3540182330, Berlin.

Qian M. & Cao P. (2005). *Scripta Mater.*, Vol. 52, 415-419, ISSN 1359-6462.

Qian M. & Das A. (2006). *Scripta Mater.*, Vol. 54, 881-886, ISSN 1359-6462.

Qian M. (2006). *Acta Mater.*, Vol. 54, 2241-2252, ISSN 1359-6454.

Qian M. & Ramirez A. (2009). *J. Appl. Phys.*, Vol. 105, 013538, ISSN 0021-8979.

Qian M., Ramirez A. & Das A. (2009). *J. Crystal Growth*, Vol. 311, 3708-3715, ISSN 0022-0248.

Qian M., Ramirez A., Das A. & StJohn D. H. (2010a). *J. Crystal Growth*, Vol. 312, 2267–2272, ISSN 0022-0248.

Qian M., Cao P., Easton M. A., McDonald S. D. & StJohn D. H. (2010b). *Acta Mater.*, Vol. 58, 3262–3270, ISSN 1359-6454.

Ramirez A. & Qian M. (2007). *Magnesium Technology 2007*, pp. 127-132, ISBN 978-0-87339-663-9, Orlando, FL, February, 2007, TMS, Warrendale, PA.

Ramirez A., Qian M., Davis B. & Wilks T. (2009). *Inter. J. Cast Metal. Res.*, Vol. 22, 260-263, ISSN 1364-0461.

Ramirez A., Qian M., Davis B., Wilks T. & StJohn D. H. (2008). *Scripta Mater.*, Vol. 59, 19-22, ISSN 1359-6462.

Sahu K. C. (1984). *Phys. Lett. A*, Vol. 102, 370-372, ISSN 0375-9601.

StJohn D. H., Qian M., Easton M. A., Cao P. & Hildebrand Z. (2005). *Metall. Mater. Trans. A*, Vol. 36, No. 7, 1669-1679, ISSN 1073-5623.

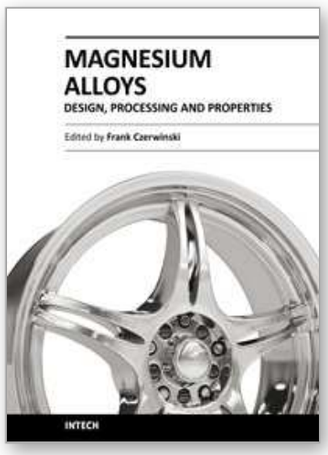
Xu Z., Yan J., Chen W. & Yang S. (2008). *Mater. Lett.*, Vol. 62, 2615-2618, ISSN 0167-577X.

Zhang X., Inada T., Yabe A., Lu S. & Kozawa Y. (2001). *Inter. J. Heat Mass Transfer*, Vol. 44, 4533-4539, ISSN 0017-9310.

Zhang Z. Q., Le Q. C. & Cui J. Z. (2007). *Mater. Sci. Forum*, Vols. 546-549, 129-132, ISSN 0255-5476.

IntechOpen

IntechOpen



Magnesium Alloys - Design, Processing and Properties

Edited by Frank Czerwinski

ISBN 978-953-307-520-4
Hard cover, 526 pages
Publisher InTech
Published online 14, January, 2011
Published in print edition January, 2011

Scientists and engineers for decades searched to utilize magnesium, known of its low density, for light-weighting in many industrial sectors. This book provides a broad review of recent global developments in theory and practice of modern magnesium alloys. It covers fundamental aspects of alloy strengthening, recrystallization, details of microstructure and a unique role of grain refinement. The theory is linked with elements of alloy design and specific properties, including fatigue and creep resistance. Also technologies of alloy formation and processing, such as sheet rolling, semi-solid forming, welding and joining are considered. An opportunity of creation the metal matrix composite based on magnesium matrix is described along with carbon nanotubes as an effective reinforcement. A mixture of science and technology makes this book very useful for professionals from academia and industry.

How to reference

In order to correctly reference this scholarly work, feel free to copy and paste the following:

Anthony Ramirez and Ma Qian (2011). Ultrasonic Grain Refinement of Magnesium and Its Alloys, Magnesium Alloys - Design, Processing and Properties, Frank Czerwinski (Ed.), ISBN: 978-953-307-520-4, InTech, Available from: http://www.intechopen.com/books/magnesium-alloys-design-processing-and-properties/ultrasonic-grain-refinement-of-magnesium-and-its-alloys

INTECH
open science | open minds

InTech Europe
University Campus STeP Ri
Slavka Krautzeka 83/A
51000 Rijeka, Croatia
Phone: +385 (51) 770 447
Fax: +385 (51) 686 166
www.intechopen.com

InTech China
Unit 405, Office Block, Hotel Equatorial Shanghai
No.65, Yan An Road (West), Shanghai, 200040, China
中国上海市延安西路65号上海国际贵都大饭店办公楼405单元
Phone: +86-21-62489820
Fax: +86-21-62489821

© 2011 The Author(s). Licensee IntechOpen. This chapter is distributed under the terms of the Creative Commons Attribution-NonCommercial-ShareAlike-3.0 License, which permits use, distribution and reproduction for non-commercial purposes, provided the original is properly cited and derivative works building on this content are distributed under the same license.

IntechOpen

IntechOpen